Six-Dimensional Atmosphere Entry Guidance based on Dual Quaternion

Conference Paper · January 2021

DOI: 10.2514/6.2021-0507

Changhuang Wan
The Ohio State University

Paige Pei
Purdue University

Ran Dai
Purdue University

Gangshan Jing
Chongqing University

Six-Dimensional Atmosphere Entry Guidance based on Dual Quaternion

Changhuang Wan *
The Ohio State University, Columbus, Ohio, 43210

Chaoying Pei †, Ran Dai ‡
Purdue University, West Lafayette, IN, 47907

Gangshan Jing §,
North Carolina State University, Raleigh, NC, 27607

Jeremy R. Rea¶
NASA Johnson Space Center, Houston, TX, 77058

This paper investigates the six-degree-of-freedom (6-DoF) entry guidance problem for the Human Mars exploration mission. For the Human-scale entry, powered descent, and landing mission, it is required to use aerodynamic forces to decelerate the vehicle during the entry phase. Instead of assuming the entry vehicle as a point mass, we consider both the translational and rotational dynamics. Specifically, the 6-DoF rigid body kinematics and dynamics of the entry vehicle are represented by unit dual quaternions, which reduces the non-linearity of dynamic equations comparing with the Euler angle based dynamical model. Moreover, the equivalence between the dual quaternion based and Euler angle based models is analyzed. Then, the optimal entry guidance problem is formulated to minimize the terminal speed subject to the dual quaternion based dynamics, operational and mission constraints, including heating rate and the normal load of the entry vehicle. By using a discretization technique and polynomial approximation, the optimal entry guidance problem is reformulated into a nonconvex quadratically constrained quadratic program (QCQP) problem, which is solved via a customized alternating direction method of multipliers (ADMM). The accuracy of the dual quaternion based model and the computational efficiency of the ADMM algorithm are verified via numerical simulations.

I. Introduction

Atmosphere entry guidance refers to the process of generating guidance commands for the hypersonic spacecraft to safely and precisely guide the vehicle from the initial state to the designed final state [1]. Due to the large and exponential variation of Mars atmosphere density, and the lack of translational controls on the vehicle, the entry guidance is recognized as a challenging task [2]. In the human Mars mission, the entry vehicle is at least ten times heavier than the one in past robotic missions [3], which makes the entry guidance even more challenging.

Extensive research has been conducted to solve the entry guidance problem. For example, work in [4] has shown that the optimal aerocapture trajectory, in general, has a bang-bang control structure, and a two-phase numerical predictor-corrector guidance algorithm has been developed. Moreover, [5] extends the predictor-corrector algorithm to a unified method that is applicable to a wide range of entry vehicles with varying lift-drag capabilities. The second-order cone programming algorithm has been applied to generate optimal paths in the entry phase [6]. Our recent work in [7] investigated the integrated entry and the powered descent guidance problem by planning the entire mission as a whole. Another work in [8] compared the performance of the Mars entry guidance results using bank angle control and direct force control, where the direct force control method has verified advantage in terms of eliminating the open-loop flight errors.

*Graduate Research Assistant, Department of Mechanical and Aerospace Engineering . wan.326@osu.edu
†Graduate Research Assistant, School of Aeronautics and Astronautics. pei.145@osu.edu
‡Assistant Professor, School of Aeronautics and Astronautics. Senior Member AIAA. dai.490@osu.edu
§Postdoctoral Research Fellow , Department of Electrical and Computer Engineering. nameisjing@gmail.com
¶Subsystem Manager, Flight Mechanics and Trajectory Design Branch, 2001 NASA Parkway - EG5; AIAA Member.

Most existing work related to entry guidance considers three-degree-of-freedom (3-DoF) dynamics. The entry vehicle can only adjust its attitude such that the aerodynamic forces can be appropriately utilized to control the speed and orientation of the vehicle during the entry phase. Although adaptive controllers have been adopted to control attitude of the entry vehicle to minimize the trajectory tracking errors, they have decoupled the translation trajectory optimization and vehicle attitude control as two problems [2, 9]. However, due to the 6-DoF aerodynamic effects, it is essential to consider the translation and rotation motion simultaneously in an entry guidance problem. The equations of motion of the entry vehicle are described using Euler angles in existing literature [1, 6, 10–13]. The trigonometric functions involved in the motion dynamics generally lead to highly nonlinear representations. As a result, it is computationally complicated to obtain an optimal/sub-optimal guidance solution with high-precision within a limited time.

This paper considers both translational and rotational motion for guidance of a human-scale entry vehicle. Moreover, to avoid the high non-linearity from Euler angle based models, the 6-DoF rigid body kinematics and dynamics of the entry vehicle are represented by dual quaternions. The equations of motion based on dual quaternions also provide a globally nonsingular representation of the rotation for a rigid body [14, 15]. To our best knowledge, it is the first time the equations of motion of the entry vehicle is modeled using dual quaternions. By combining the dual quaternion based entry dynamics with mission and operational constraints, the entry guidance problem is formulated as an optimal control problem to minimize the final speed within a specified altitude range. To solve the resulting optimal control problem, we firstly approximate all non-polynomial functions, e.g., the atmosphere density model, by continuous or piecewise continuous polynomials. Then, via discretization techniques, the optimal control problem is reformulated as a polynomial programming problem. Due to the fact that a polynomial program can be expressed as an equivalent nonconvex quadratically constrained quadratic programming (QCQP) problem by introducing new variables and quadratic constraints, we eventually represent the entry guidance problem using a unified formulation, named general/nonconvex QCQP. A customized alternating direction method of multipliers (ADMM) developed in [7] is applied to solve the formulated QCQP. The customized ADMM significantly reduces computational efforts required to solve every iterative subproblem, which is applicable to this large-scale optimal control problem. To verify the effectiveness of the dual quaternion based entry guidance model and efficiency of the customized ADMM algorithm, simulation examples with comparative results from Euler angle based model and nonlinear programming (NLP) solvers are provided at the end.

The rest of the paper is organized as follows. §II introduces the formulation of the entry guidance problem based on dual quaternion. §III presents the equivalence analysis of dual quaternion and Euler angle based models. §IV briefly describes conversion from the optimal control into a homogeneous QCQP, and the framework of the customized ADMM to search for the optimal solution of general/nonconvex QCQPs. §V provides simulation results. Conclusions are addressed in §VI.

II. Problem Formulation

A. Introduction of Dual Quaternion

A quaternion $\hat{\mathbf{q}}$ is represented by a scalar q_0 and a vector $\mathbf{q} = [q_1, q_2, q_3]^T$, namely,

$$\hat{\mathbf{q}} = q_0 + \mathbf{q} \in \mathbb{H}, \tag{1}$$

where $\mathbb{H}$ denotes the set of quaternions. The quaternion can be viewed as a 4-tuple (q_0, q_1, q_2, q_3). Quaternions whose real part is zero are called *pure quaternions*, and a quaternion is called a *unit quaternion* if its norm is 1. Unit quaternions are usually used to describe orientations and rotations of an object in three dimensions [16].

Dual quaternion is an extension of quaternion to efficiently express both rotation and translation between two coordinate frames [17]. A dual quaternion $\tilde{\boldsymbol{\sigma}}$ has the form

$$\tilde{\boldsymbol{\sigma}} = \hat{\mathbf{p}} + \epsilon\hat{\mathbf{q}} \in \mathbb{Q}, \tag{2}$$

where ϵ is the dual unit which has the property $\epsilon^2 = 0$, $\mathbb{Q}$ denotes the set of dual quaternions, and $\hat{\mathbf{p}}$, $\hat{\mathbf{q}} \in \mathbb{H}$ are given as $\hat{\mathbf{p}} = p_0 + \mathbf{p}$ and $\hat{\mathbf{q}} = q_0 + \mathbf{q}$, respectively. We can also view $\tilde{\boldsymbol{\sigma}}$ as an 8-tuple: $(p_0, p_1, p_2, p_3, q_0, q_1, q_2, q_3)$.

Let's define $\tilde{\boldsymbol{\sigma}}_1$ and $\tilde{\boldsymbol{\sigma}}_2$ to be two dual quaternions, written as

$$\tilde{\boldsymbol{\sigma}}_1 = \hat{\mathbf{p}}_1 + \epsilon\hat{\mathbf{q}}_1, \quad \tilde{\boldsymbol{\sigma}}_2 = \hat{\mathbf{p}}_2 + \epsilon\hat{\mathbf{q}}_2. \tag{3}$$

Then we have the dual quaternion operations below

$$\text{Scaler multiplication:} \quad s\tilde{\boldsymbol{\sigma}}_1 = s\hat{\mathbf{p}}_1 + \epsilon(s\hat{\mathbf{q}}_1) \tag{4a}$$

$$\text{Addition:} \quad \tilde{\boldsymbol{\sigma}}_1 + \tilde{\boldsymbol{\sigma}}_2 = \hat{\mathbf{p}}_1 + \hat{\mathbf{p}}_2 + \epsilon(\hat{\mathbf{q}}_1 + \hat{\mathbf{q}}_2) \tag{4b}$$

$$\text{Multiplication:} \quad \tilde{\boldsymbol{\sigma}}_1 \otimes \tilde{\boldsymbol{\sigma}}_2 = \hat{\mathbf{p}}_1 \otimes \hat{\mathbf{p}}_2 + \epsilon(\hat{\mathbf{p}}_1 \otimes \hat{\mathbf{q}}_2 + \hat{\mathbf{p}}_2 \otimes \hat{\mathbf{q}}_1) \tag{4c}$$

$$\text{Cross product:} \quad \tilde{\boldsymbol{\sigma}}_1 \oslash \tilde{\boldsymbol{\sigma}}_2 = \hat{\mathbf{p}}_1 \oslash \hat{\mathbf{p}}_2 + \epsilon(\hat{\mathbf{p}}_1 \oslash \hat{\mathbf{q}}_2 + \hat{\mathbf{q}}_1 \oslash \hat{\mathbf{p}}_2) \tag{4d}$$

$$\text{Conjugate:} \quad \tilde{\boldsymbol{\sigma}}^* = \hat{\mathbf{p}}^* + \epsilon\hat{\mathbf{q}}^* \tag{4e}$$

$$\text{Norm:} \quad \|\tilde{\boldsymbol{\sigma}}\| = \sqrt{\tilde{\boldsymbol{\sigma}} \otimes \tilde{\boldsymbol{\sigma}}^*} \tag{4f}$$

B. Definition of Coordinate Frames

To describe the motion of spacecraft in the entry phase, the following five coordinate frames are defined as below:

1. Inertial Coordinate Frame $\mathscr{I} - O_I X_I Y_I Z_I$: The origin O_I locates at the center of Mars, $O_I Z_I$ points to the North Pole direction. $O_I X_I$ and $O_I Y_I$ are in the Equatorial plane and determined by the right-hand rule.

2. Mars-fixed Coordinate Frame $\mathscr{M} - O_M X_M Y_M Z_M$: The origin O_M locates at the center of Mars, and the $\mathscr{M}$ frame rotates with Mars. Here we assume that the rotation of Mars is ignored. Thus $\mathscr{M}$ frame will coincide with $\mathscr{I}$ frame.

3. Vehicle-pointing Coordinate Frame $\mathscr{P} - O_P X_P Y_P Z_P$: The origin O_P locates at the center of Mars, and the X_P axis-positive is in the direction of position vector $\vec{\boldsymbol{r}}$; Y_P axis locates in the equatorial plane, vertical to X_P axis and pointing to the East; Z_P axis is perpendicular to the $X_P - Y_P$ plane with positive determined by the right-hand rule.

4. Body Coordinate Frame $\mathscr{B} - O_B X_B Y_B Z_B$: The origin O_B locates at the vehicle's center of gravity, X_B axis-positive points the nose of the aircraft in the plane of symmetry of the landing vehicle; Z_B axis is perpendicular to the X_B axis, in the plane of symmetry of the spacecraft, positive upon the aircraft; Y_B axis is perpendicular to the $X_B - Z_B$ plane with positive determined by the right-hand rule.

5. Wind Coordinate Frame $\mathscr{W} - O_W X_W Y_W Z_W$: The origin O_W locates at the gravity center, Y_W axis-positive is in the direction of the velocity vector of the craft relative to the air; X_W axis positive is in the same direction as the projection of the lift force on the plane determined by X_P and velocity of the vehicle, Z_W axis is perpendicular to the $X_W - Y_W$ plane with positive determined by the right-hand rule.

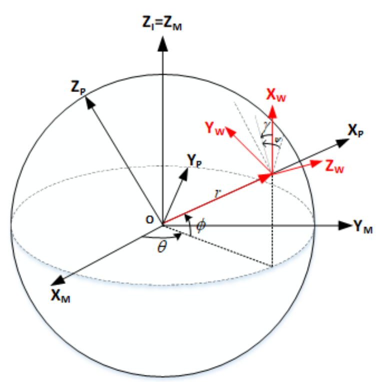

Fig. 1 Coordinate Frames Definition

In addition, in this paper, we make the following two assumptions:

Assumption II.1. *Since the entry phase is operated in a relatively short duration (compared with Mars day), the rotation of Mars is ignored.*

Assumption II.2. *The aerodynamic center can be regarded as fixed on the vehicle at low angles of attack.*

C. Equation of Motion based on Dual Quaternions

1. 6-DoF Kinematics

We use the following dual quaternion components to denote the rotation and translation between Mars frame $\mathscr{M}$ and body frame $\mathscr{B}$

$$\tilde{\mathbf{q}} = \begin{bmatrix} \hat{\mathbf{q}}_\mathrm{r} \\ \hat{\mathbf{q}}_\mathrm{d} \end{bmatrix} = \begin{bmatrix} \hat{\mathbf{q}}_\mathrm{r} \\ \frac{1}{2}\hat{\mathbf{t}}_M \otimes \hat{\mathbf{q}}_\mathrm{r} \end{bmatrix}, \tag{5}$$

where $\hat{\mathbf{q}}_\mathrm{d} \in \mathbb{H}$ denotes a translation $\hat{\mathbf{t}}_M \in \mathbb{H}$, expressed in the Mars frame $\mathscr{M}$, followed by a rotation $\hat{\mathbf{q}}_\mathrm{r} \in \mathbb{H}$ with $\|\hat{\mathbf{q}}_\mathrm{r}\| = 1$. Accordingly, the time derivatives of the dual quaternion elements can be written as

$$\dot{\tilde{\mathbf{q}}} = \frac{1}{2}\tilde{\mathbf{q}} \otimes \tilde{\mathbf{w}}, \tag{6}$$

where $\tilde{\mathbf{w}} = [\hat{\omega}, \hat{\mathbf{v}}_M] \in \mathbb{Q}$, and $\hat{\omega}, \hat{\mathbf{v}}_M$ are pure quaternions representing the angular velocity and the linear velocity of the vehicle, respectively.

2. 6-DoF Dynamics

In the entry phase, the dynamics is expressed as

$$\frac{d}{dt}(m\mathbf{v}_B) = m\dot{\mathbf{v}}_B + \boldsymbol{\omega}_B \times m\mathbf{v}_B = \mathbf{g}_B + \mathbf{F}_B, \tag{7a}$$

$$\frac{d}{dt}(\mathbf{J}\boldsymbol{\omega}_B) = \mathbf{J}\dot{\boldsymbol{\omega}}_B + \boldsymbol{\omega}_B \times m\boldsymbol{\omega}_B = \mathbf{r}_\mathrm{w} \times \mathbf{F}_B + \mathbf{M}_B, \tag{7b}$$

where $\boldsymbol{\omega}_B \in \mathbb{R}^3$ is the projection of angular velocity of the vehicle on the body frame, $\mathbf{v}_B \in \mathbb{R}^3$ is the projection of velocity on the body frame, m denotes the mass of the vehicle, $\mathbf{r}_\mathrm{w} \in \mathbb{R}^3$ denotes the constant body-frame vector from the vehicle's center of mass to the aerodynamic center, $\mathbf{F}_B \in \mathbb{R}^3$ represents the aerodynamic forces expressed in body frame, $\mathbf{g}_B \in \mathbb{R}^3$ is the gravity expressed in the body frame, $\mathbf{J} \in \mathbb{R}^{3\times3}$ represents the general inertia matrix of the entry vehicle, and $\mathbf{M}_B = [M_x, M_y, M_z]^T \in \mathbb{R}^3$ is the vector of moments that are treated as controls. Combining the two equations above, we can rewrite the dynamics using dual quaternions

$$\mathbf{J}_\mathrm{d}\dot{\tilde{\mathbf{w}}} + \tilde{\mathbf{w}} \oslash \mathbf{J}_\mathrm{d}\tilde{\mathbf{w}} = \boldsymbol{\Phi}\tilde{\mathbf{F}}_B + \tilde{\mathbf{G}}_B + \tilde{\mathbf{M}}_B, \tag{8}$$

where

$$\mathbf{J}_\mathrm{d} = \left[\begin{array}{cc|c} \multicolumn{2}{c|}{\mathbf{0}_{4\times4}} & m\mathbf{I}_4 \\ \hline 1 & \mathbf{0}_{1\times3} & \\ \mathbf{0}_{3\times1} & \mathbf{J} & \mathbf{0}_{4\times4} \end{array}\right]_{8\times8} \in \mathbb{R}^{8\times8}, \quad \boldsymbol{\Phi} = \left[\begin{array}{c|c} & \mathbf{I}_3 \\ & \mathbf{0}_{1\times3} \\ \mathbf{0}_{8\times5} & \mathbf{r}_\mathrm{w} \\ & \mathbf{0}_{1\times3} \end{array}\right]_{8\times8} \in \mathbb{R}^{8\times8}, \quad \tilde{\mathbf{F}}_B = \left[\begin{array}{c} \mathbf{0}_{4\times1} \\ \hline 0 \\ \mathbf{F}_B \end{array}\right]_{8\times1} \in \mathbb{Q},$$

$$\tilde{\mathbf{G}}_B = \left[\begin{array}{c} 0 \\ \mathbf{g}_B \\ \hline \mathbf{0}_{4\times1} \end{array}\right]_{8\times1} \in \mathbb{Q}, \qquad \tilde{\mathbf{M}}_B = \left[\begin{array}{c} \mathbf{0}_{4\times1} \\ \hline 0 \\ \mathbf{M}_B \end{array}\right]_{8\times1} \in \mathbb{Q}.$$

Here, $\mathbf{I}_n$ is the n-dimensional identity matrix. Based on the definition of coordinate frames, the gravity and aerodynamic forces can be easily described in the vehicle-pointing frame $\mathscr{P}$ and the wind frame $\mathscr{W}$, respectively. Specifically, the dual quaternion of gravity force in $\mathscr{P}$ is written as

$$\tilde{\mathbf{G}}_P = [\mathbf{0}_{1\times4}, 0, -mg, 0, 0]^T \in \mathbb{Q}, \tag{9}$$

where $g \in \mathbb{R}$ is the gravitational acceleration. Then, we have the relationship between $\tilde{\mathbf{G}}_P$ and $\tilde{\mathbf{G}}_B$, expressed as

$$\tilde{\mathbf{G}}_B = \tilde{\mathbf{q}}_\mathrm{pb}^* \otimes \tilde{\mathbf{G}}_P \otimes \tilde{\mathbf{q}}_\mathrm{pb}, \tag{10}$$

where $\tilde{\mathbf{q}}_{\mathrm{pb}} \in \mathbb{Q}$ denotes the rotation and translation from $\mathscr{P}$ to $\mathscr{B}$ frame. Similarly, the dual quaternion of the aerodynamic forces in the wind frame $\mathscr{W}$ can be written as

$$\tilde{\mathbf{F}}_W = [\mathbf{0}_{1\times 4},\, 0, -D, 0, L]^T = [\mathbf{0}_{1\times 4},\, 0, -\frac{1}{2}c_D \rho S V^2, 0, \frac{1}{2}c_L \rho S V^2]^T \in \mathbb{Q}, \tag{11}$$

where $\rho \in \mathbb{R}$ is the Mars atmosphere density, $L \in \mathbb{R}$ and $D \in \mathbb{R}$ are the lift and drag forces, $S \in \mathbb{R}$ is the reference area, $V \in \mathbb{R}$ is the velocity magnitude, and $c_L \in \mathbb{R}$, $c_D \in \mathbb{R}$ respectively denote the lift and drag coefficients of the vehicle. Moreover, c_L and c_D are linear and quadratic functions of angle of attack α, expressed as

$$c_L = c_{l_0} + c_{l_1}\alpha,\;\; c_D = c_{d_0} + c_{d_1}\alpha + c_{d_2}\alpha^2, \tag{12}$$

where $c_{l_0}, c_{l_1}, c_{d_0}, c_{d_1}, c_{d_2}$ are constant coefficients. Similar to (10), we have

$$\tilde{\mathbf{F}}_B = \tilde{\mathbf{q}}_{\mathrm{bw}} \otimes \tilde{\mathbf{F}}_W \otimes \tilde{\mathbf{q}}_{\mathrm{bw}}^* \in \mathbb{Q}, \tag{13}$$

where $\tilde{\mathbf{q}}_{\mathrm{bw}} \in \mathbb{H}$ denotes the dual quaternion from $\mathscr{B}$ to $\mathscr{W}$ frame, which is defined as

$$\tilde{\mathbf{q}}_{\mathrm{bw}} = \begin{bmatrix} \hat{\mathbf{q}}_{\mathrm{bw}} \\ \frac{1}{2}\hat{\mathbf{r}}_{\mathrm{w}} \otimes \hat{\mathbf{q}}_{\mathrm{bw}} \end{bmatrix}, \tag{14}$$

where $\hat{\mathbf{r}}_{\mathrm{w}} \in \mathbb{H}$ is a pure quaternion expressed as $\hat{\mathbf{r}}_{\mathrm{w}} = [0, \mathbf{r}_{\mathrm{w}}]$. In fact, all four components in quaternion $\hat{\mathbf{q}}_{\mathrm{bw}}$ are determined by two rotational angles (α, β), expressed as

$$\hat{\mathbf{q}}_{\mathrm{bw}} = \begin{pmatrix} q_{\mathrm{bw}_1} \\ q_{\mathrm{bw}_2} \\ q_{\mathrm{bw}_3} \\ q_{\mathrm{bw}_4} \end{pmatrix} = \begin{pmatrix} \cos\frac{\alpha}{2}\cos\frac{\beta}{2} \\ \sin\frac{\alpha}{2}\cos\frac{\beta}{2} \\ \cos\frac{\alpha}{2}\sin\frac{\beta}{2} \\ -\cos\frac{\alpha}{2}\sin\frac{\beta}{2} \end{pmatrix}, \tag{15}$$

where β is the side-slip angle. Then, $\tilde{\mathbf{F}}_W$ can be expressed with respect to the dual angular velocity $\tilde{\mathbf{w}}$, written as

$$\tilde{\mathbf{F}}_W = \frac{1}{2} S\rho V^2 \Omega \left[\begin{array}{c} \mathbf{0}_{4\times 1} \\ \hline 0 \\ -c_D \\ 0 \\ c_L \end{array}\right] = \frac{1}{2} S\rho \|\mathbf{A}\tilde{\mathbf{w}}\|^2 \Omega, \tag{16}$$

where

$$\mathbf{A} = \left[\begin{array}{c|c} \mathbf{0}_{4\times 4} & \mathbf{0}_{4\times 4} \\ \hline \mathbf{0}_{4\times 4} & \mathbf{I}_4 \end{array}\right]_{8\times 8} \in \mathbb{R}^{8\times 8},\;\; \Omega = \left[\begin{array}{c|cccc} \mathbf{0}_{4\times 4} & & \mathbf{0}_{4\times 4} & & \\ \hline & 0 & 0 & 0 & 0 \\ \mathbf{0}_{4\times 4} & 0 & -c_D & 0 & 0 \\ & 0 & 0 & 0 & 0 \\ & 0 & 0 & 0 & c_L \end{array}\right]_{8\times 8} \in \mathbb{R}^{8\times 8}.$$

D. Operational and Mission Constraints

For safe operation, specific operational and mission constraints during the entry phase are considered, including

1) Stagnation-point convective heating load constraint

$$\dot{Q} = k_Q \sqrt{\frac{\rho}{R_{\mathrm{nose}}}} V^{3.15} \le \dot{Q}_{\max}, \tag{17}$$

where $R_{\mathrm{nose}} \in \mathbb{R}$ is the nose radius of the vehicle, $k_Q \in \mathbb{R}$ is a constant depending on the composition of the Martian atmosphere, $\dot{Q}_{\max} \in \mathbb{R}$ denotes the allowable peak heating rate. This inequality constrains the heating rate at a stagnation point on the surface of the vehicle with a curvature radius R_{nose} [5].

2) Normal load constraint

$$\|\hat{\mathbf{F}}_W\| = \sqrt{L^2 + D^2} \leq n_{\max}, \tag{18}$$

where $n_{\max} \in \mathbb{R}$ is the allowable normal load on the surface of the entry vehicle.

3) Upper and lower bounds of controls

$$M_x^L \leq M_x \leq M_x^U,\ M_y^L \leq M_y \leq M_y^U,\ M_z^L \leq M_z \leq M_z^U. \tag{19}$$

E. Additional Constraints

According to (5), the dual quaternion $\tilde{\mathbf{q}}$ can be divided into two parts $\hat{\mathbf{q}}_\mathrm{r}$ and $\hat{\mathbf{q}}_\mathrm{d}$, where $\hat{\mathbf{q}}_\mathrm{r}$ represents the rotation from $\mathscr{M}$ frame to $\mathscr{B}$ frame. Here we introduce $\hat{\mathbf{q}}_\mathrm{mp} \in \mathbb{H}$ to represent the rotation from $\mathscr{M}$ frame to $\mathscr{P}$ frame, and $\hat{\mathbf{q}}_\mathrm{pb} \in \mathbb{H}$ to represent the rotation from $\mathscr{P}$ frame to $\mathscr{B}$ frame. Then according to Euler's rotation theorem, we have

$$\hat{\mathbf{q}}_\mathrm{mp} \otimes \hat{\mathbf{q}}_\mathrm{pb} = \hat{\mathbf{q}}_\mathrm{r}. \tag{20}$$

Next we try to find the constraints on $\hat{\mathbf{q}}_\mathrm{mp}$ based on the expression of $\hat{\mathbf{t}}_M$, which can be expressed as $\hat{\mathbf{t}}_M = [0, \mathbf{t}_M]$. Here, $\mathbf{t}_M \in \mathbb{R}^3$ is the vector from the origin of $\mathscr{M}$ frame to the origin of $\mathscr{B}$ frame projected on the $\mathscr{M}$ frame, and it can be expressed as $\mathbf{t}_M = [t_{M_1}, t_{M_2}, t_{M_3}]^T$. According to (5), $\hat{\mathbf{t}}_M$ can be written as

$$\hat{\mathbf{t}}_M = 2\hat{\mathbf{q}}_\mathrm{d} \otimes \hat{\mathbf{q}}_\mathrm{r}^*. \tag{21}$$

Alternatively, when projecting $\hat{\mathbf{t}}_M$ on the $\mathscr{P}$ frame, we can obtain $\hat{\mathbf{t}}_P = [0, r, 0, 0]^T \in \mathbb{H}$, where $r \in \mathbb{R}$ is the radial distance between the vehicle and the center of Mars. With (21) and $\hat{\mathbf{q}}_\mathrm{mp}$, we have

$$\hat{\mathbf{t}}_M = \hat{\mathbf{q}}_\mathrm{mp} \otimes \hat{\mathbf{t}}_P \otimes \hat{\mathbf{q}}_\mathrm{mp}^*. \tag{22}$$

Thus, combining (21) and (22), we can obtain $r = \|2 \cdot \hat{\mathbf{q}}_\mathrm{d}\|$.

Proposition II.3. *The dynamical system defined in* (5)-(16) *and* (20)-(22) *is self-contained. That is, it can be written in the form* $\dot{\mathbf{x}} = f(\mathbf{x})$*, where* $\mathbf{x} \in \mathbb{R}^\mathbf{n}$ *includes all unknown state variables.*

Proof. It is obvious that $\tilde{\mathbf{q}}$, $\tilde{\mathbf{w}}$, $\hat{\mathbf{F}}_B$, $\hat{\mathbf{G}}_B$, $\hat{\mathbf{q}}_\mathrm{pb}$, $\hat{\mathbf{t}}_M$, and $\hat{\mathbf{q}}_\mathrm{bw}$ can all be updated by constraints (5)-(16) and (20)-(22). We only have to show that $\hat{\mathbf{q}}_\mathrm{mp}$ can also be updated based on $\tilde{\mathbf{q}}$, $\tilde{\mathbf{w}}$, $\hat{\mathbf{F}}_B$, $\hat{\mathbf{G}}_B$, $\hat{\mathbf{q}}_\mathrm{pb}$, $\hat{\mathbf{t}}_M$, and $\hat{\mathbf{q}}_\mathrm{bw}$. From (22), it holds that

$$\begin{pmatrix} 0 \\ t_{M_1} \\ t_{M_2} \\ t_{M_3} \end{pmatrix} = \hat{\mathbf{q}}_\mathrm{mp} \otimes \hat{\mathbf{t}}_P \otimes \hat{\mathbf{q}}_\mathrm{mp}^* = \begin{pmatrix} q_{\mathrm{mp}_1} \\ q_{\mathrm{mp}_2} \\ q_{\mathrm{mp}_3} \\ q_{\mathrm{mp}_4} \end{pmatrix} \otimes \begin{pmatrix} 0 \\ r \\ 0 \\ 0 \end{pmatrix} \otimes \begin{pmatrix} q_{\mathrm{mp}_1} \\ -q_{\mathrm{mp}_2} \\ -q_{\mathrm{mp}_3} \\ -q_{\mathrm{mp}_4} \end{pmatrix} = \begin{pmatrix} 0 \\ r(q_{\mathrm{mp}_1}^2 + q_{\mathrm{mp}_2}^2 - q_{\mathrm{mp}_3}^2 - q_{\mathrm{mp}_4}^2) \\ 2r(q_{\mathrm{mp}_1} q_{\mathrm{mp}_4} + q_{\mathrm{mp}_2} q_{\mathrm{mp}_3}) \\ 2r(q_{\mathrm{mp}_2} q_{\mathrm{mp}_4} - q_{\mathrm{mp}_1} q_{\mathrm{mp}_3}) \end{pmatrix}. \tag{23}$$

Since $\hat{\mathbf{q}}_\mathrm{mp}$ is determined by the longitude $\theta \in \mathbb{R}$ and latitude $\phi \in \mathbb{R}$. Then $\hat{\mathbf{q}}_\mathrm{mp}$ can be written as

$$\hat{\mathbf{q}}_\mathrm{mp} = \begin{pmatrix} \cos\frac{\theta}{2}\cos\frac{\phi}{2} \\ \sin\frac{\theta}{2}\cos\frac{\phi}{2} \\ \sin\frac{\theta}{2}\sin\frac{\phi}{2} \\ -\cos\frac{\theta}{2}\sin\frac{\phi}{2} \end{pmatrix} \tag{24}$$

Substituting (24) into (23), we can obtain the relationships below

$$t_{M_1} = r\cos\phi, \quad t_{M_2} = -r\cos\theta\sin\phi, \quad t_{M_3} = -r\sin\theta\sin\phi. \tag{25}$$

Then ϕ and θ can be determined by

$$\phi = \arccos(\tfrac{t_{M_1}}{r}), \quad \theta = \arccos(-\tfrac{t_{M_2}}{r\cos\phi}). \tag{26}$$

With given θ and ϕ, $\hat{\mathbf{q}}_\mathrm{mp}$ is determined accordingly. $\square$

F. Formulation of the Optimal Guidance Problem

In this subsection, we organize the above constraints during the entry guidance and formulate the guidance problem as an optimal control problem. The objective is to minimize the terminal velocity magnitude within a specified altitude range. Combining all constraints, the optimal control problem for entry phase guidance is formulated as

$$
\begin{aligned}
&\min_{M_x, M_y, M_z, t_f} \|\mathbf{A}\tilde{\mathbf{w}}(t_f)\|, \qquad (27)\\
&\text{subject to } \dot{\tilde{\mathbf{q}}} = \frac{1}{2}\tilde{\mathbf{q}} \otimes \tilde{\mathbf{w}}, \mathbf{J}_\mathrm{d}\dot{\tilde{\mathbf{w}}} + \tilde{\mathbf{w}} \oslash \mathbf{J}_\mathrm{d}\tilde{\mathbf{w}} = \Phi\tilde{\mathbf{F}}_B + \tilde{\mathbf{G}}_B + \tilde{\mathbf{M}}_B,\\
&\tilde{\mathbf{G}}_P = [\mathbf{0}_{1\times 4} \mid 0, -mg, 0, 0]^T,\ \tilde{\mathbf{G}}_B = \tilde{\mathbf{q}}_\mathrm{pb}^* \otimes \tilde{\mathbf{G}}_P \otimes \tilde{\mathbf{q}}_\mathrm{pb},\\
&\tilde{\mathbf{F}}_B = \tilde{\mathbf{q}}_\mathrm{wb}^* \otimes \tilde{\mathbf{F}}_W \otimes \tilde{\mathbf{q}}_\mathrm{wb},\ \tilde{\mathbf{F}}_W = \frac{1}{2}\rho S \|\mathbf{A}\tilde{\mathbf{w}}\|^2 \Omega,\ \tilde{\mathbf{q}} = \tilde{\mathbf{q}}_\mathrm{mp} \otimes \tilde{\mathbf{q}}_\mathrm{pb},\\
&c_D = c_{d_0} + c_{d_1}\alpha + c_{d_2}\alpha^2,\ \ c_L = c_{l_0} + c_{l_1}\alpha,\\
&\dot{Q} = k_Q\sqrt{\frac{\rho}{R_\mathrm{nose}}}V^{3.15} \le \dot{Q}_\mathrm{max},\ \|\mathbf{F}_W\|_2 \le n_\mathrm{max},\\
&M_x^L \le M_x \le M_x^U,\ M_y^L \le M_y \le M_y^U,\ M_z^L \le M_z \le M_z^U,\\
&\tilde{\mathbf{q}}(t_0) = \tilde{\mathbf{q}}_0,\ \tilde{\mathbf{w}}(t_0) = \tilde{\mathbf{w}}_0,\ R_f^L \le \|\tilde{\mathbf{q}}(t_f)\| \le R_f^U,
\end{aligned}
$$

where t_0, t_f are respectively the starting and final time of the entry phase, R_f^L and R_f^U are respectively the lower and upper bounds for the terminal radial distance.

III. Equivalence between Dual Quaternion based Model and Euler Angle based Model

Since the dual quaternion based entry kinematics and dynamics is the first time introduced for entry guidance, we will demonstrate the equivalence between the dual quaternion based model and the traditional Euler angle based Model.

A. Entry Translational Motion based on Euler Angle

The dimensionless equations of motion based on Euler angles for the entry phase are expressed as

$$\dot{r} = V\sin(\gamma), \tag{28a}$$

$$\dot{\theta} = \frac{V\cos\gamma\cos\psi}{r\cos\phi}, \tag{28b}$$

$$\dot{\phi} = \frac{V\cos\gamma\sin\psi}{r}, \tag{28c}$$

$$\dot{V} = -D - \frac{V\sin\gamma}{r^2}, \tag{28d}$$

$$\dot{\gamma} = \frac{1}{V}(L\cos\sigma + (V^2 - \frac{1}{r})\frac{\cos\gamma}{r}), \tag{28e}$$

$$\dot{\psi} = \frac{L\sin\sigma}{V\cos\gamma} - \frac{V\cos\gamma\cos\psi\tan\phi}{r} \tag{28f}$$

where $\gamma \in \mathbb{R}$ and $\psi \in \mathbb{R}$ represent flight-path angle and heading angle, $\sigma \in \mathbb{R}$ is the bank angle to be controlled. In this model, the rotation of the vehicle is not taken into consideration. Thus, we will present the equivalence between the translation part of the dual quaternion based model in (6)-(8) and the Euler angle based model in (28).

B. Equivalence of Translational Kinematics

In this section, from the dual quaternion expressions, we will demonstrate the equivalence entry motion kinematics based on Euler angles. We start with finding the connections between $\hat{\mathbf{q}}_\mathrm{d}$, $\hat{\mathbf{t}}_M$, $\hat{\mathbf{v}}_M$ and θ, ϕ, γ, ψ, r, V. In the vehicle pointing frame, we have $\hat{\mathbf{t}}_P = [0, r, 0, 0]^T$. Thus, $\hat{\mathbf{t}}_M$ can be expressed as:

$$\hat{\mathbf{t}}_M = [0, r\cos\phi\cos\theta, r\cos\phi\sin\theta, r\sin\phi]^T. \tag{29}$$

Recall that in the wind frame $\mathscr{W}$, the velocity of a vehicle in the quaternion form is denoted by $\hat{\mathbf{v}}_W = [0,0,V,0]^T$, we then have

$$\hat{\mathbf{v}}_M = \hat{\mathbf{q}}(\theta,\phi) \otimes \hat{\mathbf{q}}(\psi,\gamma) \otimes \hat{\mathbf{v}}_W \otimes \hat{\mathbf{q}}^*(\psi,\gamma) \otimes \hat{\mathbf{q}}^*(\theta,\phi) \tag{30}$$

From (29), $\hat{\mathbf{t}}_M$ can be obtained from

$$\dot{\hat{\mathbf{t}}}_M = \begin{pmatrix} 0 \\ \dot{r}\cos\phi\cos\theta - \dot{\phi}r\sin\phi\sin\theta - \dot{\theta}r\cos\phi\sin\theta \\ \dot{r}\cos\phi\sin\theta - \dot{\phi}r\sin\phi\sin\theta + \dot{\theta}r\cos\phi\cos\theta \\ \dot{r}\sin\phi + \dot{\phi}r\cos\phi \end{pmatrix} = \begin{pmatrix} 0 \\ \dot{\mathbf{t}}_M \end{pmatrix}. \tag{31}$$

Since $\dot{\mathbf{t}}_M = \mathbf{v}_M$, we have

$$\hat{\mathbf{q}}^*(\theta,\phi) \otimes \dot{\hat{\mathbf{t}}}_M \otimes \hat{\mathbf{q}}(\theta,\phi) = \hat{\mathbf{q}}(\psi,\gamma) \otimes \hat{\mathbf{v}}_W \otimes \hat{\mathbf{q}}^*(\psi,\gamma) = \begin{pmatrix} 0 \\ V\sin\gamma \\ V\cos\gamma\cos\psi \\ V\cos\gamma\sin\psi \end{pmatrix}. \tag{32}$$

Also note that

$$\hat{\mathbf{q}}^*(\theta,\phi) \otimes \dot{\hat{\mathbf{t}}}_M \otimes \hat{\mathbf{q}}(\theta,\phi) = \begin{pmatrix} 0 \\ R_y(\phi)R_z^T(\theta)\dot{\mathbf{t}}_M \end{pmatrix} = \begin{pmatrix} 0 \\ \dot{r} \\ \dot{\theta}r\cos\phi \\ \dot{\phi}r \end{pmatrix}, \tag{33}$$

where $\mathbf{R_y}(\phi) = \begin{pmatrix} \cos\phi & 0 & \sin\phi \\ 0 & 1 & 0 \\ -\sin\phi & 0 & \cos\phi \end{pmatrix}$, $\mathbf{R_z^T} = \begin{pmatrix} \cos\theta & \sin\theta & 0 \\ -\sin\theta & \cos\theta & 0 \\ 0 & 0 & 1 \end{pmatrix}$. According to the equivalence between (32) and (33), we have $\dot{r} = V\sin\gamma$, $\dot{\theta} = \frac{V\cos\gamma\cos\psi}{r\cos\phi}$, $\dot{\phi} = \frac{V\cos\gamma\sin\psi}{r}$. By this step, we verify the equivalence of kinematics based on dual quaternions and Euler angle expressions.

C. Equivalence of Translational Dynamics

When considering force elements in different frames, (7a) can be written in different forms. For example, the most convenient way to write the relative velocity is in the wind frame, i.e., $\hat{\mathbf{v}}_W = [0,V,0,0]^T$, while the simplest way to express the angular velocity term is in the Inertia frame or Mars frame, i.e., $\hat{\boldsymbol{\omega}}_I = [0,0,0,0]^T \in \mathbb{H}$. Considering the relationships between different frames, we select the vehicle pointing frame $\mathscr{P}$ to express all forces. Then in frame $\mathscr{P}$, we have

$$\frac{d}{dt}(m\mathbf{v}_P) = m\dot{\mathbf{v}}_P + \boldsymbol{\omega}_P \times m\mathbf{v}_P = \mathbf{g}_P + \mathbf{F}_P, \tag{34}$$

where $\mathbf{F}_P = \mathbf{L}_P + \mathbf{D}_P \in \mathbb{R}^3$. To verify the equivalence of dynamics between quaternion and Euler angle expressions, we will find each force component expressed in frame $\mathscr{P}$. In the wind frame $\mathscr{W}$, the lift force $\hat{\mathbf{L}}_W = [0, L\cos\sigma, 0, L\sin\sigma]^T \in \mathbb{H}$ is perpendicular to the velocity vector $\mathbf{v}_W$. The direction of the drag is in the opposite direction of the velocity vector, i.e., $\hat{\mathbf{D}}_W = [0,0,-D,0]^T \in \mathbb{H}$. We can obtain $\hat{\mathbf{F}}_W = [0, L\cos\sigma, -D, L\sin\sigma]^T \in \mathbb{H}$ and $\hat{\mathbf{F}}_P \in \mathbb{H}$ is expressed as

$$\hat{\mathbf{F}}_P = \hat{\mathbf{q}}(\psi,\gamma) \otimes \hat{\mathbf{F}}_W \otimes \hat{\mathbf{q}}^*(\psi,\gamma) = \begin{bmatrix} 0 \\ \begin{pmatrix} 1 & 0 & 0 \\ 0 & \cos\psi & -\sin\psi \\ 0 & \sin\psi & \cos\psi \end{pmatrix} \begin{pmatrix} \cos\gamma & \sin\gamma & 0 \\ -\sin\gamma & \cos\gamma & 0 \\ 0 & 0 & 1 \end{pmatrix} \begin{pmatrix} L\cos\sigma \\ -D \\ L\sin\sigma \end{pmatrix} \end{bmatrix}. \tag{35}$$

In the $\mathscr{P}$ frame, the gravity force can be expressed as $\hat{\mathbf{g}}_P = [0, -mg, 0, 0]^T$. The velocity vector $\mathbf{v_P}$ can be written as in the quaternion form

$$\hat{\mathbf{v}}_P = [0, V\sin\gamma, V\cos\gamma\cos\psi, V\cos\gamma\sin\psi]^T. \tag{36}$$

If we ignore the self rotation of Mars, the angular velocity of the vehicle-pointing system $\hat{\omega}_P$ is its angular velocity with respect to Mars, which is determined by

$$\hat{\omega}_P = \begin{pmatrix} 0 \\ \begin{pmatrix} \cos\phi & 0 & -\sin(-\phi) \\ 0 & 1 & 0 \\ \sin(-\phi) & 0 & \cos\phi \end{pmatrix}\begin{pmatrix} 0 \\ 0 \\ \dot{\theta} \end{pmatrix} \end{pmatrix} + \begin{pmatrix} 0 \\ 0 \\ -\dot{\phi} \\ 0 \end{pmatrix} = \begin{pmatrix} 0 \\ \dot{\theta}\sin\phi \\ -\dot{\phi} \\ \dot{\theta}\cos\phi \end{pmatrix}, \tag{37}$$

With relationships derived in (34)-(37), substituting the corresponding terms in (28b), (28c), and(28e) leads to the following three equations

$$\frac{L\cos\gamma\cos\sigma - D\sin\gamma - mg}{m} = \dot{V}\sin\gamma + V\cos\gamma\cdot\dot{\gamma} - \frac{V^2\cos^2\gamma}{r}; \tag{38}$$

$$\begin{aligned}\frac{-L\sin\gamma\cos\psi\cos\sigma - L\sin\psi\sin\sigma - D\cos\gamma\cos\psi}{m} &= \dot{V}\cos\gamma\cos\psi - V\sin\gamma\cos\psi\cdot\dot{\gamma} - V\cos\gamma\sin\psi\cdot\dot{\psi} \\ &+ \frac{V^2\sin\gamma\cos\gamma\cos\psi}{r} - \frac{V^2\cos^2\gamma\sin\psi\cos\psi\tan\phi}{r}; \end{aligned} \tag{39}$$

$$\begin{aligned}\frac{-L\sin\gamma\sin\psi\cos\sigma + L\cos\psi\sin\sigma - D\cos\gamma\sin\psi}{m} &= \dot{V}\cos\gamma\sin\psi - V\sin\gamma\sin\psi\cdot\dot{\gamma} + V\cos\gamma\cos\psi\cdot\dot{\psi} \\ &+ \frac{V^2\sin\gamma\cos\gamma\sin\psi}{r} + \frac{V^2\cos^2\gamma\cos^2\psi\tan\phi}{r}. \end{aligned} \tag{40}$$

Let (39)$\cdot\cos\psi$+(40)$\cdot\sin\psi$, we have

$$\frac{-L\sin\gamma\cos\sigma - D\cos\gamma}{m} = \dot{V}\cos\gamma - V\sin\gamma\cdot\dot{\gamma} + \frac{V^2\sin\gamma\cos\gamma}{r}. \tag{41}$$

Let (38)$\cdot\sin\gamma$+(41)$\cdot\cos\gamma$, we have

$$\frac{-D - mg\sin\gamma}{m} = \dot{V}. \tag{42}$$

Substituting (42) into (41), it follows

$$\dot{\gamma} = \frac{1}{V}\left(\frac{L\cos\sigma}{m} + (V^2 - gr)\frac{\cos\gamma}{r}\right). \tag{43}$$

Substituting (42) and (43) into (40), we obtain

$$\dot{\psi} = \frac{L\sin\sigma}{mV\cos\gamma} - \frac{V\cos\gamma\cos\psi\tan\phi}{r}. \tag{44}$$

Then, let r, V, t be normalized by R_m, $\sqrt{g_0 R_m}$, $\sqrt{R_m/g_0}$, respectively. L and D are normalized by mg_0. Here, R_m is the radius of Mars and g_0 is the gravitational acceleration on Mars. Then, the dimensionless equation of motion in (28) can be obtained by substituting the normalized r, V, t, L and D in to (42)-(44). By this step, we verify the equivalence of dynamics based on dual quaternions and Euler angle expressions.

IV. Formulation Conversion and Framework of Customized ADMM

A. Discretization and Conversion into QCQP

In the dual quaternion based entry guidance problem formulated in (27), most constraints are formulated as quadratic functions, except those involving non-polynomial terms, including the exponential terms in the heating load constraint and the atmosphere density model. These non-polynomial functions will be approximated by high order polynomials with acceptable fitting errors. Specifically, the nonlinear atmosphere density is approximated using a six-order polynomial with the maximum error of 1e-4, expressed as

$$\rho = \sum_{i=0}^{n=6} p_i h^i, \tag{45}$$

where $p_i, i = 0, \cdots, 6$ are the fitting coefficients, and $h = (r - R_m) = \|\tilde{\mathbf{q}}\| - R_m$ is the altitude. For the heating rate bound constraint in (17), it can be rewritten as

$$V \leq \sqrt[3.15]{\frac{\dot{Q}_{\max}}{k_Q \sqrt{\rho / R_{\text{nose}}}}} := V_{\max}. \tag{46}$$

Similarly, $V_{\max}$ can be approximated by a fourth-order polynomial function,

$$V_{\max} = \sum_{i=0}^{n=4} u_i h^i, \tag{47}$$

where $u_i, i = 0, \cdots, 4$ are the fitting coefficients.

Through the approximations in (45) and (47), the entry guidance problem in (27) can be reformulated as a polynomial optimal control problem. According to [18], a polynomial optimal control problem can be converted into a polynomial programming problem via discretization techniques. Then, by introducing extra variables and quadratic constraints, it can be equivalently reformulated as a homogeneous QCQP. The general expression of QCQP is written as

$$\begin{aligned} \min_{\mathbf{x} \in \mathbb{R}^n} \ & \mathbf{x}^T \mathbf{Q}_0 \mathbf{x} \\ \text{subjecto to } & \mathbf{x}^T \mathbf{Q}_i \mathbf{x} = c_i, \ i \in \mathcal{E} \\ & \mathbf{x}^T \mathbf{P}_j \mathbf{x} \leq d_j, \ j \in \mathcal{I} \end{aligned} \tag{48}$$

where $\mathbf{x} \in \mathbb{R}^n$ is the unknown vector to be determined, $\mathbf{Q}_0 \in \mathbb{R}^{n \times n}$, $\mathbf{Q}_i \in \mathbb{R}^{n \times n}$, $i \in \mathcal{E}$, and $\mathbf{P}_j \in \mathbb{R}^{n \times n}$, $j \in \mathcal{I}$ are real systematic matrices which are unnecessary to be positive semidefinite. $\mathcal{E}$ and $\mathcal{I}$ are the indices sets of equality and inequality constraints, respectively. Due to the indefiniteness of $\mathbf{Q}_i$ or $\mathbf{P}_j$, problem (48) is generally nonconvex and NP-hard to solve. In the following, a customized ADMM, which was proposed in our previous work [7], will be applied to solve the resulting nonconvex QCQP. To keep this paper complete, the framework of the customized ADMM proposed in [7] is briefly described below.

B. Framework of Customized ADMM

In order to solve the resulting QCQP in (48), we first transform it into a consensus-constrained optimization problem formulated as

$$\begin{aligned} \min_{\mathbf{x}, \mathbf{y}} \ & \mathbf{x}^T \mathbf{Q}_0 \mathbf{y} \\ \text{subjecto to } & \mathbf{x}^T \mathbf{Q}_i \mathbf{y} = c_i, i \in \mathcal{E} \\ & \mathbf{x}^T \mathbf{P}_j \mathbf{y} \leq d_j, j \in \mathcal{I} \\ & \mathbf{x} = \mathbf{y}. \end{aligned} \tag{49}$$

Let $\boldsymbol{\nu} \in \mathbb{R}^n$, $\boldsymbol{\mu} \in \mathbb{R}^{|\mathcal{E}|}$, $\boldsymbol{\lambda} \in \mathbb{R}^{|\mathcal{I}|}$ be the Lagrange multipliers associated with the consensus constraint, equality constraints, and inequality constraints in (49), respectively. The augmented Lagrangian for (49) can be written as

$$\mathcal{L}_{\mathbf{p}}(\mathbf{x}, \mathbf{y}, \Lambda) = \mathbf{x}^T \mathbf{Q}_0 \mathbf{y} + \boldsymbol{\nu}^T (\mathbf{x} - \mathbf{y}) + \frac{\zeta_1}{2} \|\mathbf{x} - \mathbf{y}\|^2$$

$$
\begin{aligned}
&+ \sum_{i \in \mathcal{E}} \left(\mu_i (\mathbf{x}^T \mathbf{Q}_i \mathbf{y} - c_i) + \frac{\zeta_2}{2} \|\mathbf{x}^T \mathbf{Q}_i \mathbf{y} - c_i\|^2 \right) \\
&+ \sum_{j \in \mathcal{I}} f_{\zeta_3} (\lambda_j, \mathbf{x}^T \mathbf{P}_j \mathbf{y} - d_j),
\end{aligned} \tag{50}
$$

where f is a logical function defined in [7], $\mathbf{p} = [\zeta_1, \zeta_2, \zeta_3]$ is the collection of the penalty coefficients associated with the augmented terms. By employing the classical ADMM framework to solve (49), the variables $\mathbf{x}$, $\mathbf{y}$ and the Lagrange multipliers Λ at step $(k+1)$ can be updated as follows

$$\mathbf{x}^{k+1} = \arg\min_{\mathbf{x}} \mathcal{L}_{\mathbf{p}^k} (\mathbf{x}, \mathbf{y}^k, \Lambda^k) \tag{51a}$$

$$\mathbf{y}^{k+1} = \arg\min_{\mathbf{y}} \mathcal{L}_{\mathbf{p}^k} (\mathbf{x}^{k+1}, \mathbf{y}, \Lambda^k) \tag{51b}$$

$$\boldsymbol{\nu}^{k+1} = \boldsymbol{\nu}^k + \zeta_1^k (\mathbf{x}^{k+1} - \mathbf{y}^{k+1}) \tag{51c}$$

$$\mu_i^{k+1} = \mu_i^k + \zeta_2^k ((\mathbf{x}^{k+1})^T \mathbf{Q}_i \mathbf{y}^{k+1} - c_i),\ \forall i \in \mathcal{E} \tag{51d}$$

$$\lambda_j^{k+1} = \max\{0, \lambda_j^k + \zeta_3^k ((\mathbf{x}^{k+1})^T \mathbf{P}_j \mathbf{y}^{k+1} - d_j)\},\ \forall j \in \mathcal{I} \tag{51e}$$

where each penalty coefficient in $\mathbf{p}^k$ is chosen as a non-decreasing positive sequence. The updates of Lagrange multipliers in (51) are straightforward. However, the updates of $\mathbf{x}$ and $\mathbf{y}$ require to solve two sequences of convex quadratic optimization problems. For the $\mathbf{x}$-update, (50) is a strongly convex function when $\mathbf{y} = \mathbf{y}^k$ and $\Lambda = \Lambda^k$ are given. Thus, the global optimum of the sequential subproblem (51a) can be derived from the first-order optimality conditions of (50), written as

$$
\begin{aligned}
\frac{\partial \mathcal{L}_{\mathbf{p}^k} (\mathbf{x}, \mathbf{y}^k, \Lambda^k)}{\partial \mathbf{x}} &= \mathbf{Q}_0 \mathbf{y}^k + \boldsymbol{\nu}^k + \zeta_1^k (\mathbf{x} - \mathbf{y}^k) + \sum_{i \in \mathcal{E}} \left(\mu_i^k \mathbf{Q}_i \mathbf{y}^k + \zeta_2^k (\mathbf{x}^T \mathbf{Q}_i \mathbf{y}^k - c_i) \mathbf{Q}_i \mathbf{y}^k \right) \\
&+ \sum_{j \in \mathcal{I}} \Gamma_{x_j}^{\,k} (\lambda_j^k \mathbf{P}_j \mathbf{y}^k + \zeta_3^k (\mathbf{x}^T \mathbf{P}_j \mathbf{y}^k - d_j) \mathbf{P}_j \mathbf{y}^k) \\
&= \mathbf{0},
\end{aligned} \tag{52}
$$

where $\Gamma_{x_j}^{\,k}$, $j \in \mathcal{I}$, is a logical function associated with the inequality constraint j at kth step, which is defined as

$$
\Gamma_{x_j}^{\,k} = \begin{cases} 0, & \lambda_j^k + \zeta_3^k ((\mathbf{x}^k)^T \mathbf{P}_j \mathbf{y}^k - d_j) \leq 0, \\ 1, & \lambda_j^k + \zeta_3^k ((\mathbf{x}^k)^T \mathbf{P}_j \mathbf{y}^k - d_j) > 0. \end{cases} \tag{53}
$$

By solving (52), we can find the close-form solution of the $\mathbf{x}$-update, expressed as

$$\mathbf{x}^{k+1} = (\mathbf{A}_x^k)^{-1} \mathbf{b}_x^k, \tag{54}$$

where $\mathbf{A}_x^k$ and $\mathbf{b}_x^k$ are defined as

$$\mathbf{A}_x^k = \zeta_1^k \mathbf{I} + \sum_{i \in \mathcal{E}} \zeta_2^k (\mathbf{Q}_i \mathbf{y}^k)(\mathbf{Q}_i \mathbf{y}^k)^T + \sum_{j \in \mathcal{I}} \Gamma_{x_j}^{\,k} \zeta_3^k (\mathbf{P}_j \mathbf{y}^k)(\mathbf{P}_j \mathbf{y}^k)^T \tag{55a}$$

$$\mathbf{b}_x^k = -\mathbf{Q}_0 \mathbf{y}^k - \boldsymbol{\nu}^k + \zeta_1^k \mathbf{y}^k - \sum_{i \in \mathcal{E}} ((\mu_i^k - \zeta_2^k c_i) \mathbf{Q}_i \mathbf{y}^k) - \sum_{j \in \mathcal{I}} (\Gamma_{x_j}^{\,k} (\lambda_j^k - \zeta_3^k d_i) \mathbf{P}_j \mathbf{y}^k) \tag{55b}$$

where $\mathbf{A}_{\mathbf{x}}^k$ is a positive definite matrix when elements in $\mathbf{p}^k$ are all positive. Similarly, with the given $\mathbf{x}^{k+1}$ and Λ^k, the close-form solution of the sequential subproblem (51b) for $\mathbf{y}$-update can be obtained from

$$\mathbf{y}^{k+1} = (\mathbf{A}_y^k)^{-1} \mathbf{b}_y^k, \tag{56}$$

where

$$\mathbf{A}_y^k = \zeta_1^k \mathbf{I} + \sum_{i \in \mathcal{E}} \zeta_2^k (\mathbf{Q}_i \mathbf{x}^{k+1})(\mathbf{Q}_i \mathbf{x}^{k+1})^T + \sum_{j \in \mathcal{I}} \Gamma_{y_j}^{\,k} \zeta_3^k (\mathbf{P}_j \mathbf{x}^{k+1})(\mathbf{P}_j \mathbf{x}^{k+1})^T, \tag{57a}$$

$$\mathbf{b}_y^k = -\mathbf{Q}_0\mathbf{x}^{k+1} + \boldsymbol{\nu}^k + \zeta_1^k\mathbf{x}^{k+1} - \sum_{i\in\mathcal{E}}((\mu_i^k - \zeta_2^k c_i)\mathbf{Q}_i\mathbf{x}^{k+1}) - \sum_{j\in\mathcal{I}}(\Gamma_{y_j}^k(\lambda_j^k - \zeta_3^k d_i)\mathbf{P}_j\mathbf{x}^{k+1}), \tag{57b}$$

$$\Gamma_{y_j}^k = \begin{cases} 0, & \lambda_j^k + \zeta_3^k((\mathbf{x}^{k+1})^T\mathbf{P}_j\mathbf{y}^k - d_j) \le 0; \\ 1, & \lambda_j^k + \zeta_3^k((\mathbf{x}^{k+1})^T\mathbf{P}_j\mathbf{y}^k - d_j) > 0. \end{cases} \tag{57c}$$

With the analytical solutions in (54) and (56) derived for subproblems (51a) and (51b), the customized ADMM for nonconvex QCQPs in (48) is summarized in Algorithm 1.

Algorithm 1 Customized ADMM for nonconvex QCQP in (48)

Input: $\mathbf{Q}_0$, $\mathbf{Q}_i$, $\mathbf{c}_i$, $i \in \mathcal{E}$, $\mathbf{P}_j$, $\mathbf{d}_j$, $j \in \mathcal{I}$, and constant parameters β, τ, ϵ
Output: Unknown vectors $\mathbf{x}$ and $\mathbf{y}$
Initialization: $\mathbf{x}^0, \mathbf{y}^0, \Lambda^0$ and penalty coefficients $\mathbf{p}^0$

```
for k = 0, 1, 2, ... do
    Calculate the logical function Γ_{x_j}^k with x^k, y^k, Λ^k;
    x^{k+1}-update using (54) with y^k, Λ^k;
    Calculate the logical function Γ_{y_j}^k with x^{k+1}, y^k, Λ^k;
    y^{k+1}-update using (56) with x^{k+1}, Λ^k;
    Update Lagrange multipliers Λ using (51c), (51d), and (51e) with x^{k+1} and y^{k+1};
    Penalty coefficients updates;
    Calculate the error vector ξ = [ ||x^{k+1} - y^{k+1}|| / ||x^{k+1}||, Σ_{i∈E} ||(x^{k+1})^T Q_i y^{k+1} - c|| / ||c||, Σ_{j∈I} (||Γ_{x_j}^k|| + ||Γ_{y_j}^k||) / 2 ]
    if ||ξ||_1 ≤ ϵ then
        break;
    end if
    k = k + 1
end for
```

V. Simulations

In this section, we present simulation results of the dual-quaternion based entry guidance problem solved by the customized ADMM algorithm and the comparative results of the Euler angle based model using NLP solver. All simulations were run in MatLab environments on a 3.6GHz Desktop with 32 GB RAM.

A. Problem Settings

The simulation presented here uses the Hypersonic Inflatable Aerodynamic Decelerator (HIAD) in [8] as the landing vehicle. As shown in Fig. 2, HIAD has a symmetric shape without back shell covers. The payload is protected by a large diameter heatshield. Thus, the angle of attack and side-slip angle ranges are limited by $-20^\circ \le \alpha \le 20^\circ$ and $-20^\circ \le \beta \le 20^\circ$ to avoid flow impingement and radiative heating effects on the payload at high angles of attack. In addition, the lift and drag coefficients of the vehicle c_L, c_D are obtained from [19]. The parameters of the vehicle are listed below:

$$\begin{aligned}
&m = 51{,}099 \text{ kg},\ S = \pi\frac{20^2}{4}\text{m}^2,\ \mathbf{J} = \text{diag}(4.3799e5, 3.9857e5, 3.9857e5)\ \text{kg}\cdot\text{m}^2, \mathbf{r}_\text{w} = [-1, 0, 0]^T, \\
&c_{d_0} = 1.556,\ c_{d_1} = -0.004114,\ c_{d_2} = -1.182,\ c_{l_0} = -0.003636,\ c_{l_1} = -0.7813, \\
&k_Q = 1.9027\times 10^{-8}\times(\sqrt{R_m g_0})^{3.15},\ Q_{\max} = 800\,\text{W/cm}^2,\ R_f^L = R_m + 7\text{km},\ R_f^U = R_m + 12\text{km}, \\
&n_{\max} = 2.5g_E,\ g_E = 9.8\,\text{m/s}^2,\ g_0 = 3.7114\,\text{m/s}^2. M_x^L = -413\ \text{N}\cdot\text{m},\ M_x^U = 413\ \text{N}\cdot\text{m}, \\
&M_y^L = -2388100\ \text{N}\cdot\text{m},\ M_y^U = 2388100\text{N}\cdot\text{m},\ M_z^L = -1412100\ \text{N}\cdot\text{m},\ M_z^U = 1412100\text{N}\cdot\text{m}
\end{aligned} \tag{58}$$

Meanwhile, the initial states of the entry mission are given as

$$h(t_0) = 100\text{km},\ V(t_0) = 4700\ \text{m/s}, \theta(t_0) = 120^\circ,\ \phi(t_0) = 40^\circ,\ \gamma(t_0) = 12.9^\circ,\ \psi(t_0) = 0,$$

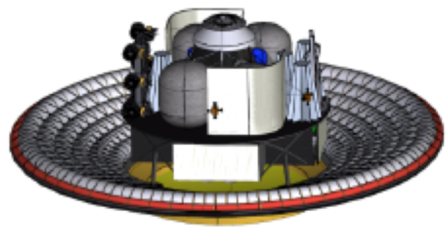

Fig. 2 Hypersonic Inflatable Aerodynamic Decelerator in [8]

$$\sigma(t_0) = -30^\circ,\ \alpha(t_0) = 17^\circ,\ \beta(t_0) = -10^\circ,\ \omega_x(t_0) = \omega_y(t_0) = \omega_z(t_0) = 0 \text{ rad/s}.$$

where ω_x, ω_y and ω_z are the angular velocities along x-, y-, z-axes, respectively. Note that the attitude angles, roll, pitch, and yaw, are determined from α and β. Then the initial states of dual quaternions $\tilde{\mathbf{q}}(t_0)$ and $\tilde{\omega}(t_0)$ can be calculated via (15)-(24) accordingly.

B. Simulation Results

By discretizing the entry phase trajectory into 31 intervals, it takes 49 iterations and 31 seconds for the customized ADMM to obtain a converged result. In comparison, it takes the NLP solver 255 iteration and 133 seconds to obtain a converged solution. The computational time from the ADMM used to solve dual quaternion based entry guidance problem significantly reduces the computational time. The optimized control and state variables are shown in Figs. 3 and 4, respectively. Obviously, the durations of the entry phase from the NLP and the ADMM are very close, namely 238.3 seconds for the NLP and 234.2 seconds for the ADMM. From Fig. 3, we know that though M_y from the NLP and the ADMM solutions have similar curves, M_x and M_z curves are different. M_x of the NLP solution switches between the upper and lower bounds frequently, whereas M_x of the ADMM solution is close to zero. Moreover, since $\mathbf{r}_w = [-1, 0, 0]^T$, there is no aerodynamic moment along x-axis. Thus, M_y and M_z have large peak values than M_x.

Figure 4a shows the altitude versus velocity curve, where the red-circle curve represents the solution from the ADMM, and the blue-star curve represents the NLP solution. The final velocity of the NLP solution is 344.7 m/s at an altitude of 7.016 km. However, the terminal velocity of the ADMM solution is 368 m/s at an altitude of 6.998km, which is slightly larger than the final velocity of the NLP solver. Additionally, both of these two curves are touching the heating rate bound at an altitude of about 45 km. Figure 4b presents time histories of α and β. Obviously, in the NLP solution, α switches between 0 and 20°, but α of the ADMM solution varies around 15° and reaches the upper bound 20° at the end of the entry phase. The side slip angle β from the ADMM solution smoothly changes from -10° to 11.29°, whereas β from the NLP switches between upper and lower bound dramatically. Similar observations are found for bank angle in Fig. 4c, as well as pitch, yaw, roll angles in Fig. 4d. Figure 4e shows the 3 dimensional trajectories of the NLP and the ADMM solutions. It can be found that the trajectories are almost overlapped at the range of high altitudes varying from 100 km to 60 km and bifurcating at around 60 km. At the end of the entry phase, the terminal latitude and longitude of the ADMM solution are 39.16° and 131.40°. The changes of latitude and longitude from the ADMM solution are larger than those from the NLP solution.

VI. Conclusions

This paper examines the six-degree-of-freedom (6-DoF) entry guidance problem that considers both translation and rotation motion. Instead of using Euler angles based dynamics, unit dual quaternion is employed to represent rigid body dynamics to reduce the non-linearity and avoid the singularity of the rotational matrix. Moreover, the equivalence between the dual quaternion based model and Euler-angle based model is analyzed. Then, combining the dual quaternion based dynamics and constraints on control and states, the 6-DoF entry guidance problem is formulated as a polynomial programming problem, which is then equivalently converted into a nonconvex quadratically constrained quadratic program (QCQP). A customized alternating direction method of multipliers is applied to solve the resulting QCQP with a convergence guarantee. Comparative simulation results are provided to validate the effectiveness of the dual quaternion based model compared to the Euler angle based model. Furthermore, the comparison also shows the improved computational efficiency of the customized ADMM algorithm in solving the entry guidance problem.

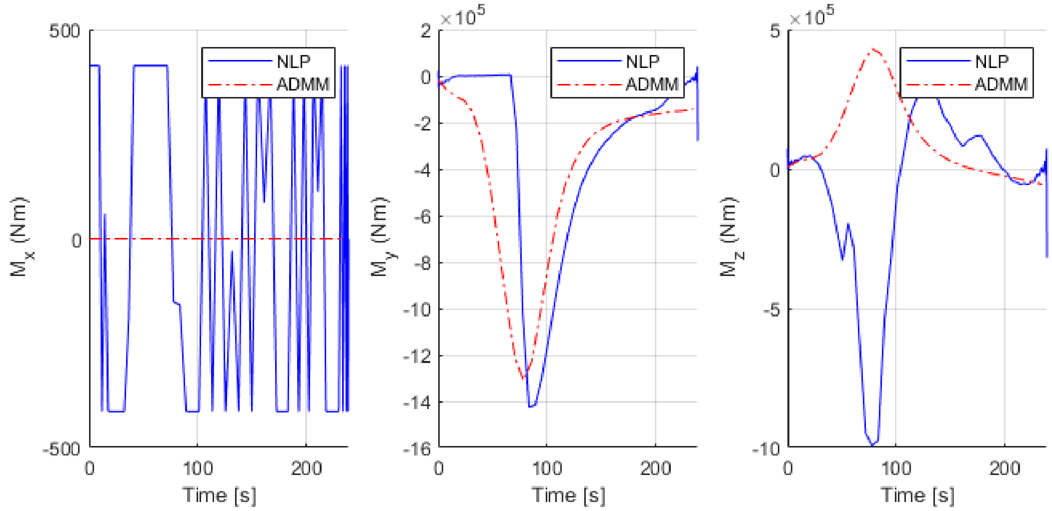

Fig. 3 Optimized controls M_x, M_y and M_z from NLP and ADMM

References

[1] Lu, P., "Entry Guidance: A Unified Method," *Journal of Guidance, Control, and Dynamics*, Vol. 37, No. 3, 2014, pp. 713–728.

[2] Restrepo, C., and Valasek, J., "Structured adaptive model inversion controller for Mars atmospheric flight," *Journal of guidance, control, and dynamics*, Vol. 31, No. 4, 2008, pp. 937–953.

[3] Cianciolo, A. D., and Polsgrove, T. T., "Human mars entry, descent, and landing architecture study overview," 2016.

[4] Lu, P., Cerimele, C. J., Tigges, M. A., and Matz, D. A., "Optimal aerocapture guidance," *Journal of Guidance, Control, and Dynamics*, Vol. 38, No. 4, 2015, pp. 553–565.

[5] Lu, P., "Entry Guidance: A Unified Method," *Journal of Guidance, Control, and Dynamics*, Vol. 37, No. 3, 2014, pp. 713–728. Doi: 10.2514/1.62605.

[6] Liu, X., Shen, Z., and Lu, P., "Entry Trajectory Optimization by Second-Order Cone Programming," *Journal of Guidance, Control, and Dynamics*, Vol. 39, 2015, pp. 1–15. https://doi.org/10.2514/1.G001210.

[7] Wan, C., Jing, G., Dai, R., and Rea, J. R., "Fuel-Optimal Guidance for End-to-End Human-Mars Entry, Powered-Descent, and Landing Mission," *AIAA Scitech 2020 Forum*, 2020, p. 1472.

[8] Dwyer Cianciolo, A., and Powell, R. W., "Entry, Descent, and Landing Guidance and Control Approaches to Satisfy Mars Human Mission Landing Criteria," 2017.

[9] Marwaha, M., and Valasek, J., "Fault-tolerant control allocation for Mars entry vehicle using adaptive control," *International Journal of Adaptive Control and Signal Processing*, Vol. 25, No. 2, 2011, pp. 95–113.

[10] Josselyn, S., and Ross, I. M., "Rapid Verification Method for the Trajectory Optimization of Reentry Vehicles," *," Journal of Guidance, Control, and Dynamics*, Vol. 26, No. 3, 2003, pp. 505–508.

[11] Bollino, K., "High-Fidelity Real-Time Trajectory Optimization for Reusable Launch Vehicles," Ph.D. thesis, 2006.

[12] Shaffer, P., Ross, I. M., Oppenheimer, M., Doman, D., and Bollino, K., "Optimal Trajectory Reconfiguration and Retargeting for Reusable Launch Vehicles," *," Journal of Guidance, Control, and Dynamics*, Vol. 30, No. 6, 2007, pp. 1794–1802.

[13] Lu, P., "Entry Guidance and Trajectory Control for Reusable Launch Vehicle," *Journal of Guidance Control and Dynamics - J GUID CONTROL DYNAM*, Vol. 20, 1997, pp. 143–149. https://doi.org/10.2514/2.4008.

[14] Lee, U., and Mesbahi, M., "Constrained Autonomous Precision Landing via Dual Quaternions and Model Predictive Control." *," Journal of Guidance Control Dynamics*, Vol. 40, No. 2, 2017, pp. 292–308.

[15] Yang, A. T., and Freudenstein, F., "Application of Dual-Number Quaternion Algebra to the Analysis of Spatial Mechanisms," *Journal of Applied Mechanics*, Vol. 31, No. 2, 1964, p. 300. https://doi.org/10.1115/1.3629601.

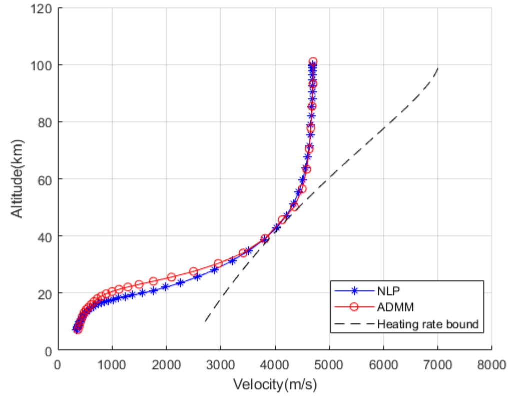

(a) Altitude vs Velocity

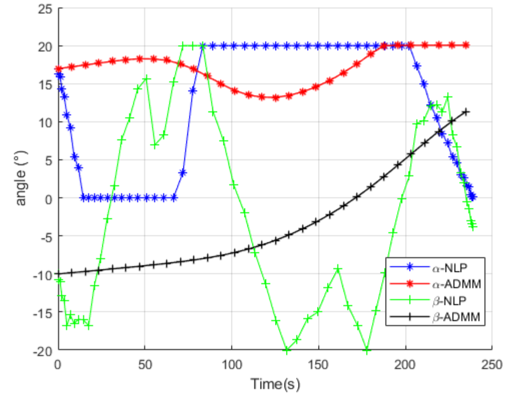

(b) Angle of attack & side-slip angle

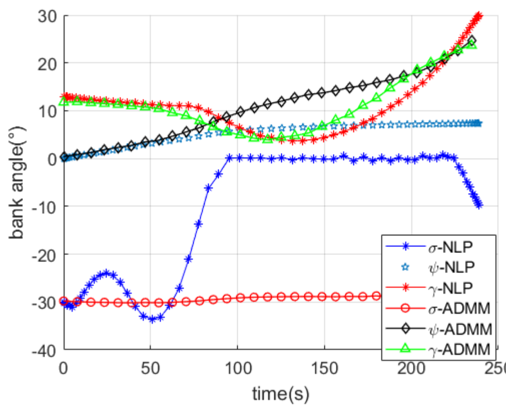

(c) Bank angle, path angle & heading angle

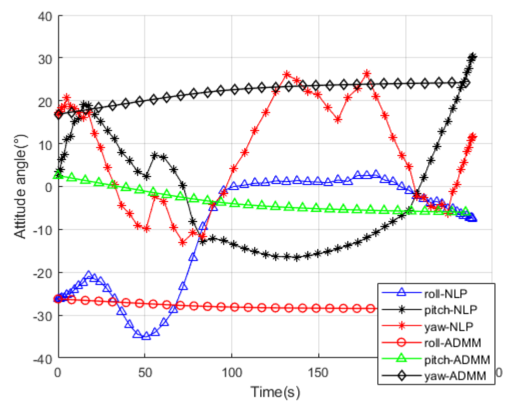

(d) Attitude angles: roll, pitch and yaw

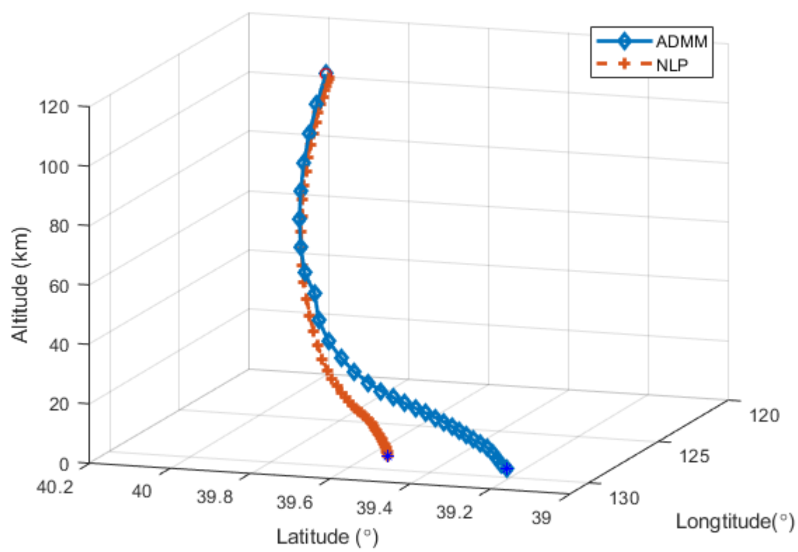

(e) Optimized 3D trajectories of NLP and ADMM

Fig. 4 State variables of converged solutions from NLP and ADMM

[16] McCarthy, J. M., *Introduction to theoretical kinematics*, MIT press, 1990.

[17] Yang, A. T., "Application of quaternion algebra and dual numbers to the analysis of spatial mechanisms," Ph.D. thesis, Columbia University Morningside Heights, New York, 1963.

[18] Wan, C., Dai, R., and Lu, P., "Alternating minimization algorithm for polynomial optimal control problems," *Journal of Guidance, Control, and Dynamics*, Vol. 42, No. 4, 2019, pp. 723–736. Doi: 10.2514/1.G003766.

[19] Harper, B. P., and Braun, R. D., "Preliminary Design Study of Asymmetric Hypersonic Inflatable Aerodynamic Decelerators for Mars Entry," *AE8900 MS Special Problems Report, Guggenheim School of Aerospace Engineering Georgia Institute of Technology Atlanta, GA*, 2014. [Online] Available: http://www.ssdl.gatech.edu/sites/default/files/ssdl-files/papers/mastersProjects/HarperB-8900.pdf.